Blindly Controlled Magnetically Actuated Capsule for Noninvasive Sampling of the Gastrointestinal Microbiome

Peyman Shokrollahi, Yung P. Lai, Samrand Rash-Ahmadi, Victoria Stewart, Mohsen Mohammadigheisar, Lee-Anne Huber, Naomi Matsuura, Anna E. H. Zavodni, John Parkinson, and Eric Diller, *Member, IEEE*

***Abstract*— *Objective:* To address the challenges of physical sample retrieval from all locations along patients' gastrointestinal (GI) tracts for studying of interactions between GI microbial communities (microbiomes) and host immune systems. *Methods:* We propose a novel tetherless, blindly controlled, magnetically actuated capsule for noninvasive sampling of GI microbiomes and liquid digesta. The mesoscale capsule, a soft mobile robot platform, is made from two permanent magnets encapsulated in a soft elastomer and actuated remotely by an external magnet. The capsule is controlled blindly using an external magnet to orient and activate the capsule. Following oral administration, capsules transit the GI tract and are activated at specified locations. The capsule is recovered via routine stool passage and collected samples are processed for downstream analyses (e.g. 16S rRNA surveys, metagenomics, metatranscriptomics and/or metabolomics). The localization of the capsule is estimated using the travelling time and the location of collected microbiomes will be confirmed by downstream analyses. A mathematical model of capsule activation is used to predict capsule activation and guide design optimization. *Results:* We demonstrate the ability of the capsule to collect samples, as well as maintain sample integrity *in vitro, ex vivo*, and with twelve capsules in *in vivo* swine models. Eleven capsules successfully collected digesta (in the range of 18 to 61 mg). *Conclusion:* The capsule successfully collected and sealed samples. *Significance:* This sampling apparatus offers a technological advance for the robust sampling of GI tract contents.**

***Index Terms*— Magnetic Actuation, Microbiome, Microrobotics, Noninvasive Sampling, Soft Robotics.**

I. Introduction

The mammalian gut is home to a complex community of microbes, termed the microbiome. Increasingly, the composition and function of the gut microbiome in humans has been linked to a large range of diseases including diabetes and inflammatory bowel disease (IBD) [1-5]. From a livestock perspective, global bans on the use of dietary supplementation of antibiotics is driving interest in the identification of alternative strategies, such as probiotic feed additives, for promoting growth through the manipulation of the gut microbiome. The key to developing new therapeutic strategies in the case of human disease, or novel feed additives in the case of livestock production, is an improved understanding of the interactions between the gut microbiome and the host immune system. A major challenge to such an understanding is the retrieval of physical samples that inform on the composition and function of the microbiome from physiologically relevant sites within the GI tract. While the composition and activity of microbes vary dramatically across the GI tract [6], [7], studies of the gut microbiome typically rely on the use of stool samples that are not reflective of intestinal sites relevant to disease or nutrient absorption.

Tethered endoscopy can be used to collect samples but is invasive, expensive, and cannot reach distal regions of the small intestine without the use of invasive tools. Complications and pain due to the disruption of the epithelium are also possible. There has thus been much interest in less invasive sampling devices for internal regions on a more regular basis [8-11].

Magnetic actuation is appealing for less invasive approaches as a low frequency magnetic field can penetrate biological tissues and fluid in the body without distortion and enables

This research was supported by the Medicine by Design New Ideas Fund MbDNI-2017-02.

P. Shokrollahi, Y.P. Lai and E. Diller are with the Department of Mechanical and Industrial Engineering, University of Toronto, Toronto, ON M5S3G8 Canada (e-mail: peyman.shokrollahi@utoronto.ca, yp.lai@mail.utoronto.ca, eric.diller@ utoronto.ca).

S. Rash-Ahmadi is with the Department of Mechanical Engineering, Urmia University, Urmia, Iran (e-mail: s.rashahmadi@urmia.ac.ir).

L. Huber, V. Stewart and M. Mohammadigheisar are with the Department of Animal Biosciences, University of Guelph, Guelph, ON, N1G2W1, Canada (email: huberl@uoguelph.ca, vstewa01@uoguelph.ca, mmohamm@uoguelph.ca).

N. Matsuura is with the Department of Materials Science and Engineering and the Institute of Biomaterials & Biomedical Engineering, University of Toronto, Toronto, ON M5S3G8 Canada (e-mail: naomi.matsuura@utoronto.ca).

A. Zavodni is with the Department of Medicine, Division of Cardiology, University of Toronto, Toronto, ON M5S 1A8 Canada (e-mail: anna.zavodni@utoronto.ca).

J. Parkinson is with the Department of Biochemistry & Molecular and Medical Genetics, University of Toronto, Toronto, ON M5S1A8 Canada (e-mail: john.parkinson@utoronto.ca).

wireless control in inaccessible regions of the body [12]. Magnetic fields have been used to apply force and torque to control a variety of medical devices inside the body. Magnetically actuated flexible endoscopes guide the tube through the intestinal tract, minimize contact with the sides of the intestines, and reduce pain and discomfort [13]. Magnetic attraction and repulsion were used to apply linear forces to a medical catheter [14], and magnetic steering was used for 3D endoscopy with a scanning catheter [15].

Magnetic actuation has been used in other tethered surgical tools in minimally invasive surgery for wireless control. Examples include catheters for laparoscopic surgery [14, 16] and tissue diagnosis [15]. A magnetic actuation mechanism does not require onboard control and power circuits [17], permitting device size downscaling and the allocation of more space for sample collection volume [18]. Several groups have developed active magnetic capsule endoscopes.

Capsule endoscopes have been developed with magnetic actuation for onboard tissue biopsy sampling by revolving blades [19,20] and needle extension [21]. However, the task of microbial sampling requires digesta fluid rather than tissue sampling, and thus a different design is required for the capsule.

Fluid sampling capsules have been envisioned using pH sensor to activate a spring [22] and heat-based melting [23] mechanisms. A micromachined capsule with motor-driven piston [24] can sample fluid but it has a risk of retention due to its size (11 × 26 mm), similar to endoscopic capsules [25, 26].

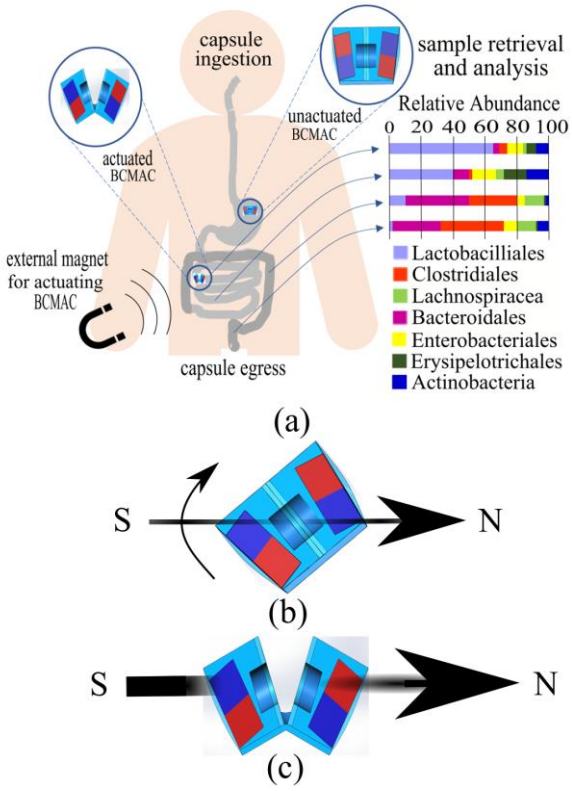

Fig. 1. The schematic of capsule operation, (a) The process of the capsule ingestion, transition, activation, egress, and sample downstream analysis, (b) alignment of the capsule with small external magnetic field, and (c) activation of capsule with a strong external magnetic field.

Existing sampling capsules contain complex onboard actuators, such as multistage valve systems [27], onboard power [24], or cutting mechanisms [19], which increases the risk of failure, poses as hazards, and limits the potential for scaling to smaller size of capsule.

TABLE I
COMPARISON OF CAPSULES OVERALL DIMENSION AND THEIR SAMPLE VOLUME

Capsule Name	Diameter (mm) × Length (mm)	Overall Volume[a] (mm^3)	Sampling Volume[b] (mm^3)
MASCE [21]	18 × 40	10179	100
Delivery/sampling system [24]	10 × 30	2356	510
Magnetic torsion spring [19]	9 × 24	1527	40
IntelliCap [27]	11 × 27	2566	300
PillCam [31]	11 × 26	2471	300
ALICE for drug delivery [28]	12 × 33	3732	-
BCMAC (current work)	**8 × 11**	**553**	**42**

[a] The overall volume was approximated based on the cylindrical shape of the capsule.
[b] The sampling volume was approximated based on the chamber volume.

Most of the developed capsule endoscopes were dedicated for imaging or drug delivery mechanisms. They do not have a requirement for sealing a sample after activation, as in the soft-magnet-based drug delivery mechanism for intestinal endoscopy and drug delivery [28] or other enhanced capsules for drug delivery [21, 29-30]. In these mechanisms, the issue of cross-contamination of samples was not considered. A capsule for drug delivery with potential for fluid sampling and imaging was designed using soft magnets for actuation about a hinge [20, 28]. However, this design required the precise knowledge of capsule orientation and position to activate the capsule. Its *in vivo* performance was not evaluated.

Furthermore, rigid capsules may be more likely to damage the lumen than a soft design. Previous sampling devices in general are not compliant [19, 22-24]. Yim's compliant magnetically actuated tetherless robot is not completely soft due to having components such as a CMOS camera, thereby the rigid exterior can cause inadvertent damage of tissues from a sharp edge in the design. This device is also a drug delivery mechanism limited to operating in the stomach [21].

No small-scale/scalable soft capsule has been developed for microbiome fluid sampling across all locations in the GI tract, with blind operation and simple sample collection mechanism. We thus propose the novel tetherless blindly controlled magnetically actuated capsule (BCMAC) for noninvasive sampling of liquid digesta containing microbiome (Fig. 1).

The BCMAC is a soft mobile robot platform comprised of two permanent magnets encapsulated in a soft elastomer with hinge and sample chamber. Following oral administration, the capsule transits the GI tract passively and is activated remotely for sampling by an external magnetic field. A patient could swallow multiple capsules (at various time points), which could be activated at once. The capsules are recovered via routine stool passage. Microbiome samples are thus encapsulated and sealed in the device during passage through the GI tract and processed upon retrieval for downstream analysis of microbiome composition and/or function (e.g. 16S rRNA

surveys, metagenomics, metatranscriptomics and/or metabolomics). Fig. 1 illustrates the concept of the capsule operation mechanism such as ingestion, alignment, activation, and egress as well as sample retrieval and analysis.

The unique advantages of the BCMAC include:

1) Smaller than other developed devices for sampling microbiomes and capable of sampling digesta along all spaces in the GI tract.

2) Capability of sealing the sample and safely transiting the sample without cross-contamination along the GI tract.

3) Less risk due to not using chemicals (e.g., electrolytes), a heating mechanism, or sharp objects (e.g., needle) in case of capsule breakage

4) Simple design with the capability of being downscaled/upscaled

5) Completely soft outer shell for a noninvasive procedure

In this paper we introduce the design and activation mechanism of the robotic capsule, introduce a mathematical model of activation, and show the device's reliable operation under application conditions, and report on *in vitro*, *ex vivo*, and *in vivo* experiments proving the sampling capability.

II. Design Specifications

Design requirements to develop the BCMAC regard size, blind activation, sealing, material strength, and biocompatibility. The following sections state the design requirements in detail and serve as an outline for the results sections of the manuscript.

A. Capsule Size and Sampling Volume

Both the overall dimension of the capsule and the collected sampling volume are critical features of the design. There is a trade-off between the overall dimension and the sampling size. A smaller capsule will more easily pass through narrow parts of the GI tract, leading to a more diverse population who can use it, in particular children [19] and IBD patients with swallowed parts [25, 26].

The upper limitation on the dimension of capsule endoscopes defined by the Food and Drug Administration (FDA) is 11 mm in diameter and 26 mm in length [19, 31]. This is a standard dimension for designing capsules to transit all spaces along the GI tract for adults and children older than 10 years [19].

The overall dimension of the capsule is critical to ensure that it can be swallowed and retrieved via stool passage. Smaller capsules are required due to non-negligible rates of retention of current endoscopic capsules with IBD [25, 26].

For suitable analysis of collected samples, a DNA or RNA concentration of roughly 100 ng/µL is enough for detection; however, this is not enough for RNA sequencing, which requires 500 ng/µL. This amount is required for the confirmatory analysis to confirm the identity of RNA [32]. With a capture volume of 42 mm^3, our device is capable of collecting 18 to 61 mg of intestinal contents. The BCMAC's sampling volume is enough for downstream analysis (e.g., 16s rRNA). With 10 mg of material capable of yielding up to 1.5 µg of DNA [33] and 4 µg of RNA [34], this provides considerably more material than required for preparation of 16S rDNA libraries as well as libraries used for whole microbiome shotgun DNA and RNA sequencing (metagenomics and metatranscriptomics respectively) [35].

B. Blind Activation

To simplify the capsule design and usage, no imaging system is used to locate the capsule. Thus, upon activation the capsule chamber must be opened blindly to collect a liquid microbiome sample (i.e., when the capsule has an unknown location and orientation within the GI tract). In the case of activating the capsule using an external magnetic field, the internal and external fields should be modeled to ensure proper activation of the capsule without damaging it. Blind activation will be tested by activating the capsule inside the GI tract without using any localization system. Given the size of the target subject, activation must be accomplished at distances defined by the body of the human or animal. The capsule will be held open for a short time (a few seconds) to ensure that a digesta sample can enter the chamber.

C. Sample Sealing

Since the collected samples are analyzed using downstream analysis, cross-contamination of samples should be avoided during the passage of the capsule before and after activation. A successful capsule seal will prevent digesta leakage in or out, thereby preventing this cross-contamination of collected samples with other liquids during capsule transition under conditions such as agitation and irregular motion. The sealing mechanism is tested by agitative motions applied to the capsule harsher than expected peristalsis motions of the GI tract.

D. Material Strength

Material strength of the compliant capsule should be sufficient for the capsule to tolerate various external and internal forces and torques, during the GI tract transit. In addition, the attraction between the two internal magnets provides the strong sealing force, which has the potential to collapse the soft chamber walls. The walls must therefore be strong enough that the capsule can be opened and closed, without damage to its parts. Strength is tested by performing tensile, agitation, and *in vivo* experiments.

E. Compatibility

Compatibility means 1) that the capsule materials in contact with GI tract tissue are acid- and enzyme-resistant, and 2) do

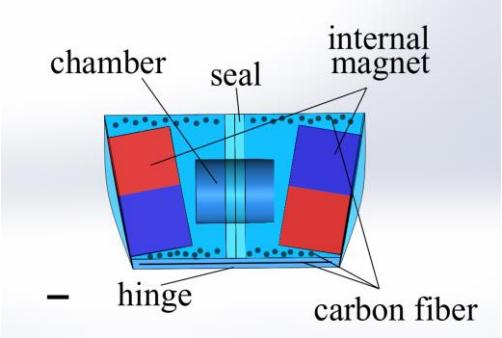

Fig. 2. The blindly controlled magnetically actuated capsule in closed state. Each of the two symmetrical sides has a chamber, internal magnet, carbon fiber, and sealing mechanism. (scale bar, 1 mm).

not biologically affect the collected samples. The capsule materials must remain intact while operating in the low-pH environment of the GI-tract with various enzymatic activity. The materials are tested in simulated digesta conditions, and a cell viability test is conducted to ensure that samples will not be affected.

III. Design and Actuation Mechanism

A. Structural Design and Actuation Mechanism

To address the engineering challenge of blind tetherless activation for noninvasive procedures, the BCMAC is designed as a compliant, small (8-mm outer diameter, 11-mm length), cylindrical silicone rubber composite capsule as shown in Fig. 2. Each of its two halves contains a disk magnet (type N52; 6 mm diameter, 3 mm thickness; magnetization direction along the diameter) and a cylindrical chamber for sample collection and storage. The two halves of the capsule are connected by a flexure hinge. Besides the magnets, the entire capsule body is made from a soft elastomer with reinforcing carbon fibers. The carbon fibers are embedded to ensure 1) the capsule does not collapse under deformation, 2) the magnets are held securely in place, and 3) the body and hinge site are reinforced.

The capsule is normally closed until an external magnetic field is applied which acts to open the capsule, as shown in Fig. 1. The applied field generates opening torque on each of the two internal magnets, acting to bring the magnets into alignment with the field. The internal magnets are oriented within the capsule such that this creates an opposite magnetic torque on each magnet, which opens the capsule. The opposite orientations of the two internal magnets also serves to generate an inter-magnet attraction force to seal the capsule. This attraction force is an important part of the design; its magnitude satisfies the capsule sealing property for safe sample transit while still allowing capsule opening with minimal external field.

For activation, the BCMAC must be aligned with the external magnetic field. To achieve this in a blind manner, the capsule is designed with a small net magnetic moment which allows the entire capsule to self-align with a small applied field prior to opening. This slight magnetic moment is created by introducing a small offset angle α_0 to the internal magnets, as seen in Fig. 3. The net magnetic moment is the summation of the two intern magnet dipole moments $\boldsymbol{m}_1$ and $\boldsymbol{m}_2$. A small external magnetic field generates a torque on this net magnetization and aligns the capsule with the external field.

Based on the orientation of the internal magnets, the external field also applies torque ($\boldsymbol{T}_{ext}$) on each magnet ($\boldsymbol{m}_1$ and $\boldsymbol{m}_2$) to open the capsule. Assume the capsule is pinned at the hinge site; the alignment of the internal magnetic moments opens the capsule. The presence of a nonzero angle α_0 also causes an internal torque ($\boldsymbol{T}_1$) between $\boldsymbol{m}_1$ and $\boldsymbol{m}_2$.

When the capsule opens, the hinge torque provides a restoring torque ($\boldsymbol{T}_h$) to re-close the capsule. Approximating the internal magnets as dipole sources, there is a magnetic force ($\boldsymbol{F}_1$) between $\boldsymbol{m}_1$ and $\boldsymbol{m}_2$ which exerts a torque around the hinge reference point and closes the capsule. Fig. 3 illustrates the forces and torques on the BCMAC halves.

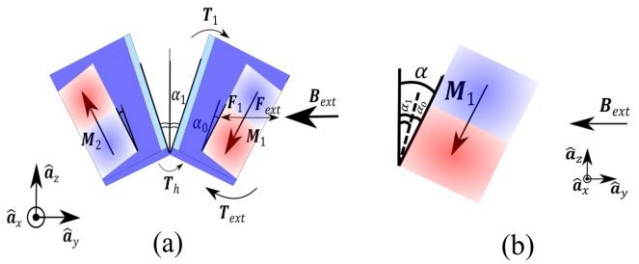

Fig. 3. A schematic of applied torques and angles. (a) Two internal permanent disk magnets show at a slanted at angle α_0, resulting in net magnetization (to the left here) when the capsule is closed. Applied magnetic torques and inter-magnet forces are shown on the right-half of the BCMAC as a free-body diagram, (b) The schematic of one internal magnet and the small offset angle (α_0), half of the opening angle (α_1), and the total angle ($\alpha = (\alpha_0 + \alpha_1)$).

When multiple capsules are fed sequentially, the capsules have the potential to clump together in the stomach as they attract each other magnetically due to their non-zero net magnetization. Thus, the capsule feeding must be spaced out in time to reduce this effect. The median gastric transit time (time to pass into the small intestine from the stomach) for endoscopic capsules is 21 min in human [36]. Capsules should thus be fed no sooner than approximately 45 min from each other. Typical GI-tract transit times in humans are 3 h for the small and 24 h for the large intestines [29].

One large external permanent magnet, or several stacked/parallel magnets [37, 38], are used for the activation, depending on the patient/animal size. This external magnet(s) is positioned by hand, which offers a flexible approach, but with risks of low precision. In this work we activate the capsule blindly by moving a permanent magnet over the body, thus exposing the entire body to the magnetic field over the duration of activation.

B. Sealing Mechanism Development

To fulfill the requirements of the sealing specifications, silicone rubber is used for the seal rim, with enough adhesion force to avoid leakage and sample contamination. This rubber is more compliant than that used in the BCMAC structure and acts as a kind of gasket. This lower stiffness rubber is created by using approximately 40% less curing catalyst than for the body silicone, which reduces the crosslinking and resulted in less stiffness.

To enhance the ability of the sampling chamber itself to fill with digesta, the inner surface of the capsule chamber is coated with a hydrophilic coating. The surface energy of this inner cavity was increased to maximize the chemical affinity with digesta and increase the collected volume. Polydopamine is used due to its ease of use, biocompatibility, and capability in cell adhesion to silicone rubber surfaces [39].

C. Reinforced Elastomer Capsule Body

Early prototypes of the capsule composed of pure elastomer tended to break apart during testing, primarily at the hinge site. The hinge is the most vulnerable part of the BCMAC; it must not break upon capsule activation. As the capsule is activated blindly at an unknown distance from the external magnet, a large external field is generally required. With a stiff hinge, a

low field cannot open the capsule. The hinge should also tolerate the large force that tries to overcome the sealing adhesion when the capsule is closed. To address the challenges of material strength, a carbon fiber is embedded in the elastomer. This creates a composite to reinforce the capsule body and hinge, providing enough strength for the hinge to tolerate the forces and torques for capsule opening. The hinge also contributes to capsule closure when the external field is removed. The developed composite provides enough strength not to open the capsule too far; beyond a certain pivot point the internal magnets stick together in the fully 'folded-back' open configuration. The use of carbon fiber embedded in the elastomer prevents the capsule halves from breaking apart on application of a strong external field.

D. Compatibility

To validate the silicone rubber compatibility, the alamarBlue (Thermo Fisher) viability test is performed for quantifying cell viability [40]. Silicone rubber samples were incubated with fibroblast media for 1, 3, and 7 days. Fibroblast cells (3×10^4 cells/well) are seeded in a 96-well plate and fed with incubated media (500 µL) for 1 day, followed by comparison with unincubated samples. To evaluate cell viability, 50 µL alamarBlue is added to each well. After 4 h incubation at 37°C in a humidified atmosphere of 5% CO_2 and 95% air, fluorescence is measured with a cyto-fluorometer adapted to a microplate (λ_{ex}: 555 nm, λ_{em}: 585 nm) using a SpectraMax i3 multimode microplate reader (Molecular Devices).

IV. Analytical Model

Capsule functionality requires control of the forces and torques involved in opening and closing. An analytical model of capsule opening is used to inform the overall design of the BCMAC system, and design parameters cannot be selected using simple intuition because of the competing nature of some of the design criteria. The model is used to explore selection and placement of internal and external magnets for proper sealing and blind opening as well as geometric design of the capsule hinge.

A. Model for the Internal Magnets

The magnetic opening torque scales with the volume of the internal magnets. Thus, the largest volume which could fit, and highest grade available were selected for them. The internal magnets can be approximated by dipole magnetic moments of $\boldsymbol{m}_1$ and $\boldsymbol{m}_2$ for the right and left side, as shown in Fig. 3. The magnetic moment is a vector pointing from the south to north magnetic pole of the internal magnet proportional to the magnet strength. The relevant magnetization vectors ($\boldsymbol{M}_1$ and $\boldsymbol{M}_2$) can be used to calculate the moments using the volume V as $\boldsymbol{m}_1 = \boldsymbol{M}_1 V$ and $\boldsymbol{m}_2 = \boldsymbol{M}_2 V$. Each magnet will experience torques and forces generated by both the other internal magnet and the external field. The torque on an internal magnet $\boldsymbol{m}$ due to an applied field $\boldsymbol{B}$ is $\boldsymbol{m} \times \boldsymbol{B}$, which acts to bring the magnetic moment into alignment with the field. The force on the magnet is created by a field spatial gradient and is $(\boldsymbol{m} \cdot \nabla)\boldsymbol{B}$, which acts approximately to move magnets towards regions of higher field strength.

The other internal magnet $\boldsymbol{m}_2$ applies internal torque $\boldsymbol{T}_1$ and force $\boldsymbol{F}_1$ to $\boldsymbol{m}_1$. The external field $\boldsymbol{B}_{ext}$ applies activating torque $\boldsymbol{T}_{ext}$ and force $\boldsymbol{F}_{ext}$ on $\boldsymbol{m}_1$. The hinge also generates a resistive torque $\boldsymbol{\tau_h}$ acting to close the capsule. These forces and torques acting on the capsule half 1 are balanced at a certain capsule opening angle α according to the torque balance equation

$$\boldsymbol{T}_1 + \boldsymbol{L} \times \boldsymbol{F}_1 + \boldsymbol{\tau}_h + \boldsymbol{m}_1 \times \boldsymbol{B}_{ext} = 0, \quad (1)$$

where $\boldsymbol{L}$ is the position vector originating from the hinge center of mass (COM) to the internal magnet COM. The angle α is the sum of the small offset angle α_0 and half of opening angle α_1 (see Fig. 3). A dipole model is used for (1) to calculate the field and its gradient generated by the internal magnet as

$$\boldsymbol{T}_1 = -\frac{\mu_0 m^2}{8\pi r^3}\sin(2\alpha)\,\hat{\boldsymbol{a}}_x \quad (2)$$

$$\boldsymbol{F}_1 = \frac{3\mu_0 m^2}{4\pi r^4}\left(-1-\sin^2(\alpha)\right)\hat{\boldsymbol{a}}_y, \quad (3)$$

where $\mu_0 = 1.257\times10^{-6}$ H/m is the magnetic permeability of free space, $m = m_1 = m_2$, r is the distance between the COMs of the internal magnets, and $\hat{\boldsymbol{a}}_x$ and $\hat{\boldsymbol{a}}_y$ are the unit vectors of the coordinate system (Fig. 3). Equation (1) can then be fully expressed as

$$\frac{\mu_0 m^2}{8\pi r^3}\sin(2\alpha)\,\hat{\boldsymbol{a}}_x + \frac{3\mu_0 L m^2}{4\pi r^4}(1+sin^2\alpha)\cos(\alpha'+\alpha_1)\,\hat{\boldsymbol{a}}_x + \left(\frac{3EI\tan(\alpha_1)}{l'}\right)\hat{\boldsymbol{a}}_x - mB_{ext}\cos(\alpha)\,\hat{\boldsymbol{a}}_x = 0, \quad (4)$$

where r is the distance between the COMs of the internal magnets, and α' is the angle between the plane intersecting both halves of the capsule and the plane passing through the COMs of the hinge and internal magnet across the capsule diagonally. The hinge torque $\boldsymbol{\tau}_h$ is approximated with the elastic model of a rectangular cantilever beam using the Euler–Bernoulli theory, where l' is the hinge length, E is the Young's modulus calculated experimentally from the results of a tensile test, and I is the second moment of area of the hinge cross section. The hinge geometrical properties (thickness and length) play critical roles in (4).

The magnitude of magnetic moment was determined as approximately 0.124 Am^2 by measuring the magnetic field it produced at various distances and fitting a dipole model. This value is comparable to the manufacturer (K&J Magnetics Inc.) reported value of 0.1178 Am^2.

The key design consideration contributing to the control of capsule opening and closing is the placement of the magnet within each half of the body, parameterized by $\boldsymbol{L}$ (position of the internal magnet relative to the hinge). Our capsule design was generated through a brute force search process by choosing $\boldsymbol{L}$ which results in sufficient sealing force but also the ability to open the capsule under the available magnetic field from the external magnet. The opening angle for the finalized design is calculated and experimentally characterized in Section VI.

B. Model for the External Magnet

The field required to open the capsule has some minimum threshold due to sealing adhesion, inter-magnet attraction within the capsule, and the hinge torque. The $\boldsymbol{B}$ field generated by the external magnet is shown in Fig. 4a for three different external magnet sizes which are commercially available and not

too large to safely handle manually. Due to the large size of the external magnet and its relatively flat rectangular shape, a dipole field model does not accurately capture the magnetic

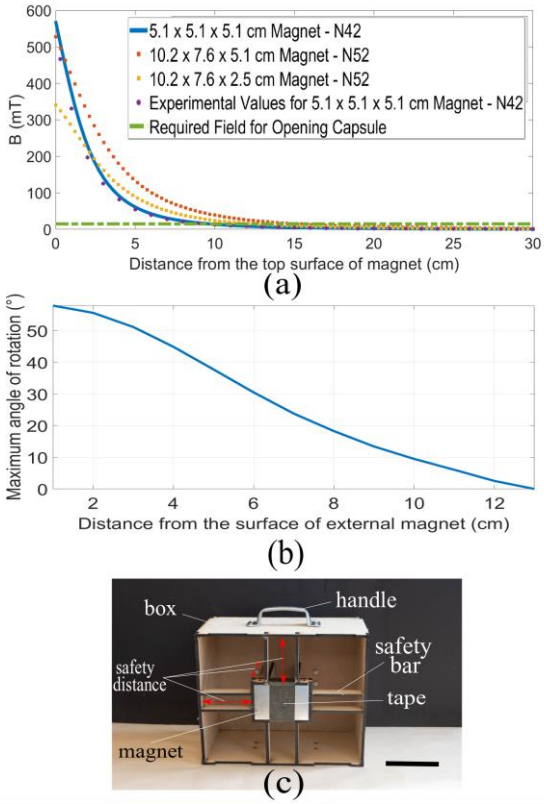

Fig. 4. (a) Calculated B-fields for three rectangular magnets using a charge model, compared with one experimental measurement. The field required to open the capsule is 15 mT (b) Maximum allowable angular misalignment of the external magnet which still results in the field strength meeting the 15 mT minimum activation threshold (c) Magnet safety box for activation, showing the magnet in the center surrounded by open space. Scale bar, 100 mm.

field at near distances from magnet. Thus, a charge model is

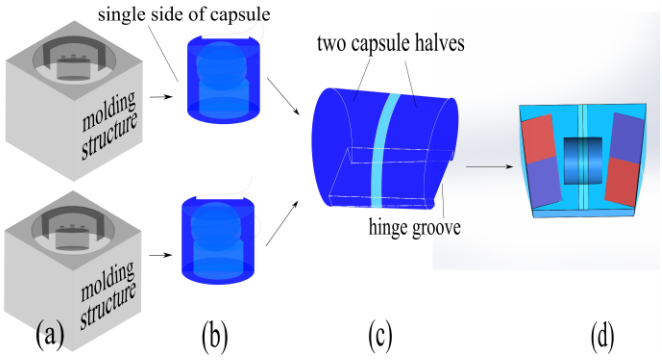

Fig. 5. The top-level schematic of the fabrication processing (a) developing couple molding structures, (b) preparing two single sides of the capsule, (c) attaching the capsule halves, and (d) fabricating the whole capsule by filling the hinge.

used. In this model, the permanent magnet is modeled as a distribution of volume (ρ_m) and surface (σ_m) magnetic charges. The volume and surface charge densities are calculated as $\rho_m = -\nabla \cdot \boldsymbol{M}$ and $\sigma_m = \boldsymbol{M} \cdot \hat{\boldsymbol{n}}$, respectively, where $\boldsymbol{M}$ is a magnetization vector and $\hat{\boldsymbol{n}}$ is a surface normal vector. Due to uniform polarization, $\boldsymbol{M} = M_S \hat{\boldsymbol{a}}_z$, thus $\rho_m = -\nabla . \boldsymbol{M} = 0$ and the model is simplified to a surface charge distribution [41]. The $\boldsymbol{B}$ field along the central axis (z) of the magnet is calculated as [41]

$$B(z) = \frac{\mu_0 M_S}{\pi}\left[tan^{-1}\left(\frac{(z+L)\sqrt{a^2+b^2+(z+L)^2}}{ab}\right) - tan^{-1}\left(\frac{z\sqrt{a^2+b^2+z^2}}{ab}\right)\right], \quad (5)$$

where a and b are the dimensions of the front surface and L is the thickness of a magnet bar. In Fig. 4a, the $\boldsymbol{B}$ field is plotted as a function of the distance (z) from the front surface.

Because the external magnet is manually controlled by hand, we also studied the effect of small angular misalignments of the external magnet from the capsule true location.

A properly aligned external magnet points the external magnet directly at the capsule. However, during blind activation of the capsule, the external magnet will be scanned systematically over the entire abdomen but will likely not point directly at the capsule when at its closest approach point. This effect is shown in Fig. 4b, where the maximum angle error from nominal is plotted as a function of the external magnet misalignment. Below this maximum angle threshold, the field will still be above the minimum required 15 mT to open the capsule at a small angle. This field was calculated experimentally, and it is confirmed through using the developed model. This is an approximation of the minimum field to open the capsule because the sealing force was not considered in this calculation.

From these results, we chose the intermediate-size external magnet (type N52, 102 × 76 × 25 mm; K&J Magnetics Inc., magnetized along its thickness) because it is easier to handle than the largest type, and still generates a large enough field for capsule activation. The external magnet is secured within a magnet safety box (Fig. 4c) for safe handling during swine testing.

V. Fabrication

In this section we describe the fabrication of the sampling capsule according to the design parameters set out in Section II. A couple similar molding structures were developed. Half of the capsule was made in each mold. Then, two capsule halves were attached through developing a hinge mechanism to from the BCMAC. Fig. 5 illustrates the top-level fabrication process. The following sections describe the fabrication process in detail.

A. Capsule Side Fabrication

A molding structure consisting of a hinge ridge, chamber ridge (creating cavities for the respective components), and magnet holders was created as outlined in Fig. 6a. A unidirectional carbon fiber fabric (2585-A; Fibre Glast Developments Corp.) was wrapped around the chamber (Fig. 6c,h). Magnets were mounted on the holders (Fig. 6d,i), designed to orient the magnets at small offset angle α_0, in the mold. Here α_0 was chosen as 10° which is a compromise between capsule activation strength and net magnetic moment strength for capsule orientation control. During curing, the

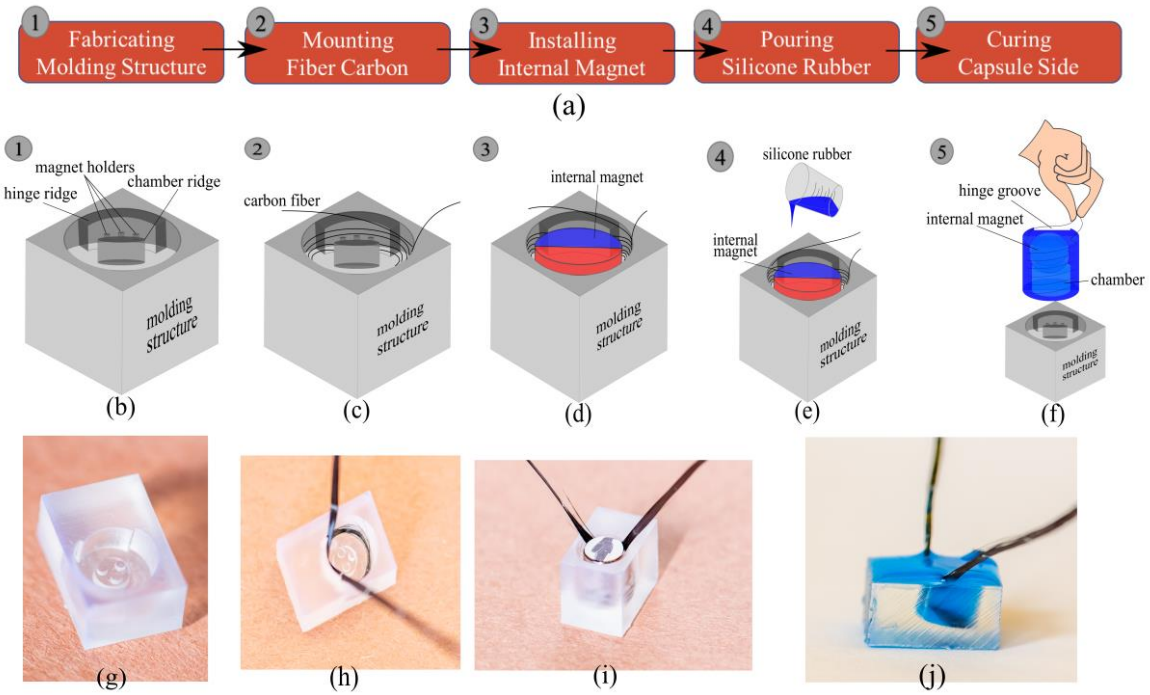

Fig. 6. (a) BCMAC fabrication steps for the two capsule halves. (b, g) The capsule end molding structure (c, h) carbon fiber mounting within the mold, (d, i) internal magnet installation, (e) pouring of silicone rubber, and (f, j) curing of the capsule sides.

internal capsule magnets were held in the correct orientation by external 25 mm cubic magnets (type N52; K&J Magnetics Inc.). The external magnet and mold were mounted on a physical fixture to maintain magnet directionality.

Silicone rubber (Mold Star 30, Smooth-On Inc.) was used at a 1:1 mass ratio of A and B parts from the manufacturer. The rubber was degassed in a vacuum chamber before and after pouring into the mold. The capsule sides were left overnight to cure.

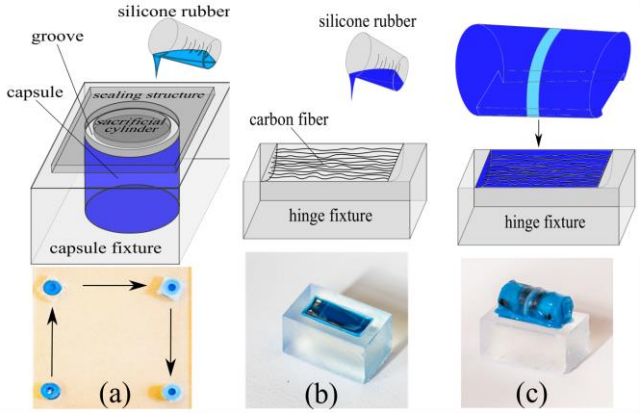

Fig. 7. (a) The four-stage process of sealing mechanism preparation, (b) mounting of carbon fiber in the hinge fixture and pouring of silicone rubber, and (c) mounting of the capsule in the hinge structure and curing of the hinge.

B. *Sealing Mechanism Fabrication*

In the capsule chamber, three orifices caused by the attachment of the magnet to the magnet holders were repaired by injection of the same silicone rubber (Mold Star 30). Then, the prepared capsule sides were mounted on a fixture for seal fabrication (Fig. 7a). A sacrificial cylinder was inserted into the chamber to form the seal geometry precisely around the rim of the capsule halves. The sealing structure and sacrificial cylinder were cubic and cylindrical laser-cut acrylic sheets with dimensions of 10 mm and diameter of 4 mm, respectively.

Degassed Mold Star 30 (10:1 mass ratio of parts A to B) was poured into the groove between the sealing structure and sacrificial cylinder and cured for 12 h. Then, the cylinder and structure were removed from the capsule side for hinge preparation.

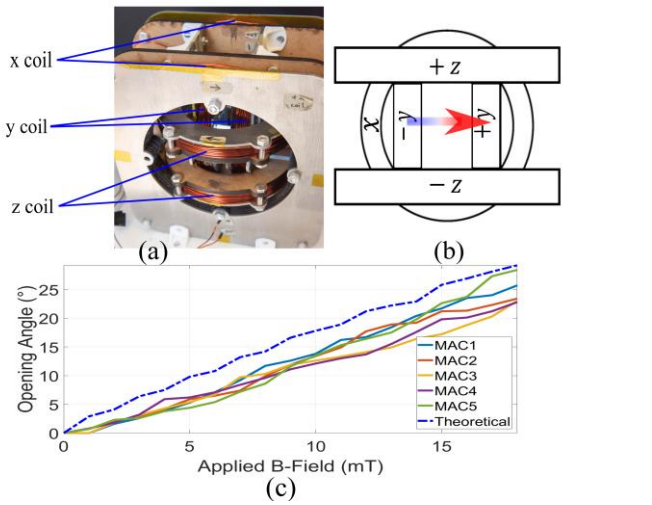

Fig. 8. (a) The Helmholtz coil used for measuring opening angles, (b) the configuration of the coils, (c) Opening angle vs. applied field for five capsules in the coil. The dashed line indicates the theoretical results derived from solving of the torque equilibrium equation. The opening angle is $2\alpha_1$ (defined in Fig. 3).

C. *Hinge Mechanism Fabrication*

For the BCMAC hinge, the composite was reinforced with the carbon fibers. Before and after fiber mounting in the hinge fixture, Mold Star 30 (1:1 mass ratio of parts A to B) was poured

into the fixture. Then, the attached capsule sides were mounted in the composite and cured overnight (Fig. 7b,c).

D. Internal Coating for Capture Enhancement

Dopamine hydrochloride (Sigma-Aldrich) was dissolved in Tris-HCl buffer (10 mM, pH 8.5 [adjusted by addition of 37% HCl]) to a concentration of 2 g/L to create the polydopamine solution as in [39]. The polydopamine solution was then placed into both sides of the capsule chamber (20 µL each) for 24 hours under air. The chambers were then flushed and washed three times with deionized water for 10 min with sonication and dried at room temperature overnight.

VI. Experiments

A. Required magnetic field for activation, capsule sealing, and capsule locomotion modes

An *in vitro* experiment was performed to determine the required magnetic field and minimum capsule–external magnet (type N52, 102 × 76 × 25 mm) distance for activation. The magnet's magnetic field was measured five times at various external magnet-to-capsule distances to determine the field required for activation. This measurement was repeated for 12 different capsules. The average distance required for activation was 53 mm, with a 15 mT field required for activation (to overcome internal torques and the adhesion caused by the sealing surfaces of the two capsule halves).

To test capsule sealing, we performed a BCMAC agitation experiment. Here 10 µL of green food dye was injected into the sampling chambers of five capsules. Each was immersed individually in 50 mL deionized water. The tubes were then agitated in a centrifuge (Sorvall Legend X1R; Thermo Scientific) at 300 rpm for 1 h at 25°C. Then, they were vortexed at maximum speed for 5 min in an analog vortex mixer (VWR International, LLC). To quantify the concentration of leaked green food dye from the capsule during this agitation, a calibration curve of five known dye concentrations (0.02, 0.01, 0.0075, 0.005, and 0 vol%) were made and the average concentration of food dye in the water of vortexed capsules was determined by UV-vis spectroscopy (Cary 50 UV-Vis spectrophotometer, Agilent Technologies). The seal was effective in preventing major leakages of dye out of the capsule (0.001 ± 0.0004 vol% dye in water after vortexing, $n = 5$).

Capsule self-alignment to an applied field was also tested in an acrylic tub container. BCMAC orienting, activating, swiveling, summersaulting, and stopping actions were tested by moving the magnet around a beaker in which the capsule was immersed in water, with the resulting motion shown in Supplementary Video 1.

B. Capsule Opening Angle Determination

To experimentally measure the opening angle of the capsule under different external magnetic field strengths, we applied fields in a Helmholtz electromagnetic coil set (Fig. 8a and 8b). In this coil pair, precise coil currents are applied by three analog servo drives (30A8; Advanced Motion Controls). Custom control code was used with a multifunction analog/digital I/O board (model 826; Sensoray) to control the coil current. Coil calibration was performed with a gaussmeter (LakeShore Cryotronics). Two cameras (FO134TC; FOculus) at the coil side and top were used at 30 frames/second to provide a view of the capsule opening motion. The coil system can generate a uniform field up to 18 mT in arbitrary three-dimensional directions near its geometric center, with ± 5% error within a 44 mm sphere.

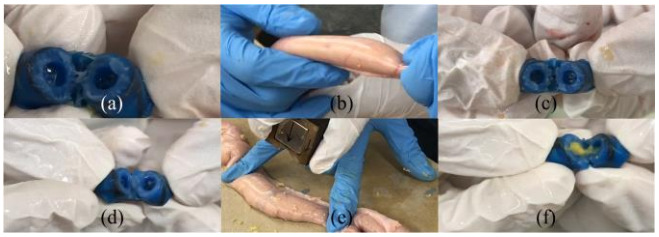

Fig. 9. (a) Inspecting capsule emptiness before insertion into the intestine section for the sealing test, (b) mechanical agitation of the intestine with the capsule inside, and (c) opening of the capsule after transit. (d) Inspecting capsule emptiness before insertion into the intestine for the activation test, e) capsule activation with a 25 mm cubic magnet, and f) inspection of digesta collection by one representative capsule.

Each of five capsules was placed in the center of the coil. Top-view images were obtained in parallel projection (i.e., parallel to the lateral capsule view) for capsule opening angle measurement. Side-view images were used to indicate the capsule position to ensure the BCMAC was in the center of the coil's workspace to ensure field uniformity. The magnetic field was applied along the capsule long axis. The capsules moved freely in contact with the bottom of the coil's working space, permitting symmetrical opening of both sides. To avoid surface tension and adhesion caused by the soft capsule seal during the opening time of the capsules, the magnetic field was first applied at 18 mT to fully open the capsule and then decreased to near zero. The opening angle as a function of applied field, reported in Fig. 8c, was identified from recorded images using the open-source Tracker software [42].

C. Materials Testing - Hydrophobicity Analysis

The capturing capability of the capsule during the activation is partially dependent on the hydrophobicity of the chamber site. To study this and assess the potential to improve the surface wettability, the contact angle of water and diiodomethane were measured on five uncoated silicone rubber samples and five coated silicone rubber samples (2 g/L dopamine in Tris-HCl buffer, 24 hours) three times each sample using a contact angle goniometer (OCA 15EC; Dataphysics). The water contact angles (mean ± SD, n = 15) were 104.5 ± 3.7° and 54.8 ± 6.0° for uncoated and coated silicone rubber, respectively. The surface energies (mean ± SD, $n = 15$), calculated as in [43], were 23.4 ± 1.4 and 44.5 ± 4.8 mN/m for uncoated and coated rubber, respectively. Polydopamine decreased the water contact angle and doubled the surface energy, providing hydrophilic coating of the silicone.

D. Materials Testing - Tensile Analysis

The silicone rubber by itself is not strong enough to hold the capsule closed during vigorous motion in the stomach of swine model. Therefore, we developed a composite reinforced with carbon fibers aligned longitudinally in the direction of the hinge as described in Section III. A tensile test was performed with two samples each of this composite and silicone rubber using

an Instron 4465 universal tensile tester with a crosshead speed of 50 mm/min, based on International Standard ISO-527. The stress-strain curves showed that the maximum tensile strength (12 MPa) of the carbon fiber composite was six times greater than that of the pure rubber (2 MPa).

E. Acid Resistivity

The biological environment of the GI tract is not hostile to silicone rubber, except in the stomach which contains hydrochloric acid with low pH < 4 [44, 45]. As the capsule may stay in the stomach for up to several hours during gastric transit, its outer shell should be acid resistant by maintaining its elastic and strength properties. To test the potential for rubber damage in acid, ten dumbbell-shaped samples were prepared according to ASTM 412-416 standard (Die C) for vulcanized rubber and thermoplastic elastomers. Five samples were immersed in hydrochloric acid (pH 1.2) for 24 h. Afterwards, the tensile properties of the 10 samples were measured using an Instron 4465 universal tensile tester with a crosshead speed of 50 mm/min, based on International Standard ISO-527.

Stress-strain curves were analyzed, where a t-test of ultimate tensile strength yielded a p value of 0.22 between samples that were exposed and those unexposed to acid, indicating no significant difference in tensile strength between acid-treated and untreated samples. No significant difference in the tangent modulus was observed and scanning electron microscope images of the rubber surface showed no discernable difference.

F. Materials Testing - Cell Viability

Cell viability on the rubber surface of the sampling chamber was tested by exposing cells to polymer for 0 (control), 1, 3, and 7 days. The percentages of cell numbers compared with the control ranged from 98% ± 0.8% (1 day) to 96% ± 0.9% (7 days). Thus, the polymer had no measurable effect on cell viability, which may be relevant to its expected effect on sampled microbiota.

G. Ex Vivo Experiments

Two meters of proximal jejunum were extracted from a freshly euthanized pig to test capsule sealing and activation. After visual inspection of their chambers to confirm they were empty, five capsules were inserted proximally into the intestine segment by hand, agitated by hand (with motion in all directions), and extracted distally. The sampling chamber contents were then examined subjectively (see Supplementary Video 2). The amount of digesta that entered into the capsules during this sealing test was insignificant.

An *ex vivo* sampling test was also conducted using the intestine segment. Each of the same five capsules was then inserted proximally, moved to the mid-jejunum, and activated using a 25 mm cubic external magnet. Then, the capsule was distally removed, and the capsule sampled content was observed (see Supplementary Video 2). In this sampling test, all five of the chambers contained significant amounts of digesta (Fig. 9f).

H. In Vivo Experiment for Digesta Sampling

To test the capability to capture samples in a live animal, *in vivo* experiments were conducted, reviewed and approved by the University of Guelph Animal Care Committee following Canadian Council on Animal Care guidelines [46]. Four capsules were fed with the aid of an injection tube in the pig's mouth to three pigs (age 7–8 weeks, body weight 15–20 kg) with a timing of 0 hr, 4 hr, 6 hr, and 8 hr. Thus 12 capsules in total were fed to the pigs. The experiments were performed on piglets with belly width of approximately 100 mm, and in that case the minimum required field was enough to activate the capsules successfully. All capsules in the pigs were activated at the same time after 30.5 h by manual motion of the external magnet around the pig abdomen. The pigs were euthanized right after the activation, to save time and reduce the risks of damage by animals, and the capsules were retrieved, immediately snap frozen at –40°C, and stored at –90°C. The content of each capsule was then weighed and used for DNA analysis. Eleven of the twelve capsules successfully collected digesta in the range of 18 to 61 mg. The twelfth capsule did not appear to open and collected no digesta sample.

VII. Discussions and Future Work

Actuation of the capsule is performed through the motion of the external magnet around the patient body. One of the limitations on activating the capsule is the distance of the capsule from the external magnet, knowing that the magnetic force is inversely proportional to the square of this distance. For blind activation of the capsule, it is required to determine the external magnet using the provided analytical model for the external magnet. Using this model, the required field and magnet properties such as dimension and type was determined for a pig with approximately 240 mm belly width. In this case, a minimum field of 15 mT required for opening the capsule should be present at minimum distance of 120 mm.

The provided capsules for the animal tests were not damaged when tested at the maximum possible field (i.e., zero distance to the external magnet). The activation distance on average was measured as 53 mm and the difference between this value and theoretical value is because the strong sealing force was not considered in the calculated theoretical value of 120 mm.

Following the above example, the dimension and type of external field can be recalculated for human belly size for a clinical purpose. The use of smaller magnets that are less dangerous are possible for the subjects with small belly widths.

The capsule's motions are not limited to alignment and activation. There is potential to drag the capsule around the location of the activation. Supplementary Video 1 also shows other locomotion control such as swiveling, summersaulting, and stopping the capsule using an external field.

An accurate model for the hinge was required to predict opening behavior of the capsule. Although an elastic model of a rectangular cantilever beam for the hinge was used for modeling the forces and torques in the capsule, it should be noted that an accurate model requires the study of nonlinear behavior of the hyper-elastic composite. However, hinge modelling will require obtaining the exact geometrical shape, length, and thickness of the hinge incorporating in deformation when the capsule is opened. The hinge behavior was complex

both in terms of material property (e.g., dimension and geometrical shape) and boundary conditions (e.g., loading, magnetic external/internal forces, internal force). In future work, a finite element model will be used to derive the behavior of the hinge during the opening of the capsule with including the internal and external magnetic forces.

The BCMAC is a device that seals the content after sampling, and safely transits the samples along the GI tract. The capsule's sealing mechanism were tested through an *in vitro* and *ex vivo* experiments. Regarding *in vitro* test for capsule sealing, the capsule was placed in harsher environment than the peristalsis motion (refer to *Supplementary Video 3*). It has been reported that peristalsis motion is mimicked in simulation using peristalsis waves [47, 48]. In these studies, pressure was used to characterize the environment effects. For example, a pressure sensing capsule endoscope was used to measure the pressure in the esophagus, stomach, intestines and colon [48]. The absolute pressure was recorded as 100.9 to 101.1 kPa in the intestines [48]. Moreover, in other papers, the maximum gastric emptying stress has been reported as approximately 10 kPa [49, 50]. The pressure exerted on the sealed capsule via centrifugation was approximated as 8.68 kPa (centrifuge speed of 300 rpm, rotor diameter of 168 mm, capsule surface area (~9.55×10^{-4} m^2, and water mass of 0.05 kg on the capsule). Higher pressures to mimic the large gastric pressures in the GI tract were unattainable due to the maximum centrifuge speed of 300 rpm of our equipment. Thus, the capsule with enclosed food dye was also vortexed. The movement of vortexing was vigorous and would exceed the stresses from gastric contractions and peristalsis movement in the human gastrointestinal tract (refer to *Supplementary* Video 3).

Regarding limitations on developing the capsule, the main limitations are on the overall dimension of the capsule, sampling size, strength of material, and activation distance. All of these limitations were considered in our design. The BCMAC is smaller than other developed devices for sampling microbiomes. Thus, the capsule can be used for sampling digesta along all spaces in the GI tract. The BCMAC has a simple structure that can be upscaled or downscaled. The upper scaling bound of the capsule is defined by the standards defined by the FDA. The lower bound can be claimed as half to third of the current size because the principles of physics do not change in this range although the fabrication of the capsule at a smaller size requires accurate instrumentations and associated with more costs.

The capturing mechanism was improved through enhancing the surface energy. A reinforced composite was also developed to have enough strength to tolerate internal magnetic forces and not damaged by the strong external field if the capsule comes into close vicinity of the external magnet. The developed analytical model can be used to calculate the required magnetic field for activating the capsule in a known subject/animal belly size. Fig. 10 displays the measured values of hinge bending deflection versus applied force. In this experiment, a load cell (GSO series, Transducer Techniques LLC, USA) was used to measure the applied force on the tip of the hinges with the same geometrical structure made up of the silicone rubber. Then the torque was evaluated based on the measured force and half of the hinge length. The theoretical values agree with measured values at small angles.

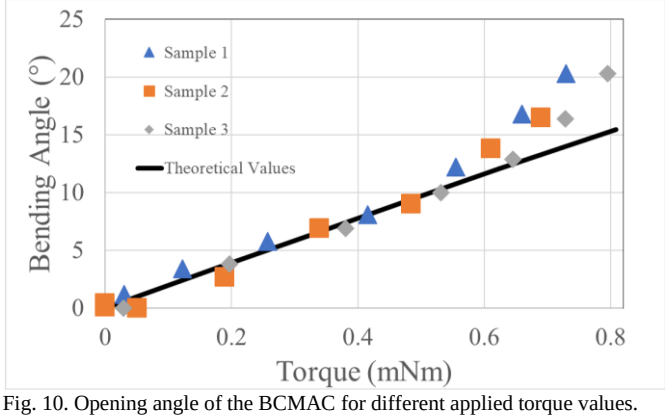

Fig. 10. Opening angle of the BCMAC for different applied torque values.

The significant contribution in this work is the use of a permanent magnet to control the BCMAC blindly. The major limitation in developing active capsules is the complexity of a coil system. The soft-magnet-based drug-delivery module for active locomotive intestinal capsule endoscopy (ALICE) has only been studied only *in vitro* because of this limitation [28]. The module uses an electromagnetic actuation (EMA) system consists of various coils required for generating uniform and gradient fields. For accommodating human or large animals in these coils, a large and complex system should be developed. Therefore, most of the developed mechanisms were only tested in *in vitro* and *ex vivo* because of the small workspace of the coil system.

The BCMAC was successfully tested *in vivo* due to using permanent magnets for the activations. The BCMAC has other differences with the soft-magnet-based drug-delivery module. In the BCMAC, the permanent magnets used to seal the capsule, always attract to enforce sealing even when the external field is not applied. This resulted in a significant difference between the measured leakage. The leakage of the dye out of the BCMAC was approximately measured as 0.001% under aggressive condition (i.e., vortexing the capsule) while the leakage of the drug-delivery module has been reported as 1.8% under stall condition (i.e., immersed into a bath) [28].

There are limitations on imaging and localizing the capsule. For future work, the capsule will be localized through incorporating an ultrasound imaging system and/or magnetic localization [51]. Preliminary tests to evaluate the potential of ultrasound tracking have been conducted. The provided Supplementary Video 4 shows the ultrasound image of capsules floating in agar gel where the magnets are highly visible (*in vitro* without magnets, with magnets, and *in vivo*). However, it is noted that there will be challenges associated with gastric gas (which reflects ultrasound) and registration of the ultrasound image with the actual location along the length of the intestine.

In conclusion, the simple sampling apparatus presented can contribute to the technological advancement required for breakthroughs in sequencing and microbial system and metabolite identification.

ACKNOWLEDGMENT

We thank Dr. Elnaz Shokrollahi for her professional photos, Doug Wey for animal tests, Tomas Bernreiter for tensile tests, Ana Popovic for data extraction, and Mohammad Mohammadi for the viability test. There is no relationship between any author and the sources of financial support for this work.

REFERENCES

[1] J. S. Biteen *et al.*, "Tools for the microbiome: nano and beyond," *ACS Nano*, vol. 10, no. 1, pp. 6–37, 2016.

[2] J. M. Kinross, A. W. Darzi, and J. K. Nicholson, "Gut microbiome-host interactions in health and disease," *Genome Med.*, vol. 3, no. 3, p. 14, 2011.

[3] (2019) Impact of IBD in Canada report. Crohn's and Colitis Canada. [Online]. Available: https://crohnsandcolitis.ca/About-Us/Resources-Publications/Impact-of-IBD-Report

[4] G. Donaldson *et al.*, "Gut biogeography of the bacterial microbiota," *Nat. Rev. Microbiol.*, vol. 14, no. 1, pp. 20–32, 2016.

[5] B. Wang *et al.*, "The human microbiota in health and disease," *Engineering*, vol. 3, no. 1, pp. 71–82, 2017.

[6] J. C. Clemente *et al.*, "The impact of the gut microbiota on human health: an integrative view," *Cell*, vol. 148, no. 6, pp. 1258–1270, 2012.

[7] G. Lv *et al.*, "The gut microbiota, tumorigenesis, and liver diseases," *Engineering*, vol. 3, no. 1, pp. 110–114, 2017.

[8] Y. Wang *et al.*, "Modulation of gut microbiota in pathological states," *Engineering*, vol. 3, no. 1, pp. 83–89, 2017.

[9] S. A. Fillon *et al.*, "Novel device to sample the esophageal microbiome–the esophageal string test," *PLoS One*, vol. 7, no. 9, e42938, 2012.

[10] D. R. F. Elliott *et al.*, "A non-endoscopic device to sample the oesophageal microbiota: a case-control study," *Lancet Gastroenterol. Hepatol.*, vol. 2, no. 1, pp. 32–42, 2017.

[11] S. M. Huse *et al.*, "Comparison of brush and biopsy sampling methods of the ileal pouch for assessment of mucosa-associated microbiota of human subjects," *Microbiome*, vol. 2, no. 1, p. 5, 2014.

[12] H. Keller *et al.*, "Method for navigation and control of a magnetically guided capsule endoscope in the human stomach," in *4th IEEE RAS & EMBS Int. Conf. on Biomed. Rob. and Biomechatronics*, Rome, Italy, 2012, pp. 859–865.

[13] G. Pittiglio *et al.*, "Magnetic levitation for soft-tethered capsule colonoscopy actuated with a single permanent magnet: A dynamic control approach," *IEEE Robot. Autom. Lett.*, vol. 4, no. 2, pp. 1224–1231, 2019.

[14] Y. Sachar and L. Farkas, "Magnetic linear actuator for deployable catheter tools," U.S. Patent 12 103 518, 2008.

[15] K.H. Kim *et al.*, "Two-axis magnetically-driven MEMS scanning catheter for endoscopic high-speed optical coherence tomography," *Optics express*, vol. 15, no. 26, pp. 18130 -18140, 2007.

[16] R.D. Brewer *et al.*, "Force control of a permanent magnet for minimally-invasive procedures," in *2nd IEEE RAS & EMBS Int. Conf. on Biomed. Rob. and Biomechatronics*, Scottsdale, AZ, USA, 2008, pp. 580–586.

[17] M. Sitti *et al.*, "Biomedical applications of untethered mobile milli/microrobots," *Proc. IEEE*, vol. 103, no. 2, pp. 205–224, 2015.

[18] A. J. Petruska and J. J. Abbott, "An omnidirectional electromagnet for remote manipulation," in *IEEE International Conference on Robotics and Automation*, Karlsruche, Germany, 2013, pp. 822–827.

[19] M. Simi, G. Gerboni, A. Menciassi, and P. Valdastri, "Magnetic torsion spring mechanism for a wireless biopsy capsule," *J. Med. Device*, vol. 7, no. 4, 2013.

[20] V.H. Le *et al.*, "Miniaturized biopsy module using gripper tool for active locomotive capsule endoscope," *Mechatronics*, vol. 44, pp. 52 – 59, 2017.

[21] S. Yim and M. Sitti, "Design and rolling locomotion of a magnetically actuated soft capsule endoscope," *IEEE Trans. Robot.*, vol. 28, no. 1, pp. 183–194, 2012.

[22] K. Kerkhof *et al.*, "Fluid Sampling Device," U.S. Patent 6333684, 2019.

[23] M. L. Jones *et al.*, "Systems and methods for obtaining samples using ingestible device," U.S. Patent 15 680 400, 2018.

[24] J. Cui *et al.*, "The study of a remote-controlled gastrointestinal drug delivery and sampling system," *Telemed. e-Health*, vol. 14, no. 7, pp. 715–719, 2008.

[25] F. Li *et al.*, "Retention of the capsule endoscope: a single-center experience of 1000 capsule endoscopy procedures," *Gastrointest. Endosc.*, vol. 68, no. 1, pp. 174–180, Jul. 2008.

[26] M. Rezapour *et al.*, "Retention associated with video capsule endoscopy: systematic review and meta-analysis," *Gastrointest. Endosc.*, vol. 85, no. 6, pp. 1157–1168.e2, 2017.

[27] D. Becker *et al.*, "Novel oral swallowable IntelliCap device to quantify regional drug absorption in human GI tract using diltiazem as model drug," *AAPS PharmSciTech*, vol. 15, no. 6, pp. 1490–1497, 2014.

[28] V. H. Le *et al.*, "A soft-magnet-based drug-delivery module for active locomotive intestinal capsule endoscopy using an electromagnetic actuation system," *Sensors and Actuators A*, vol. 243, pp. 81–89, 2016.

[29] F. Munoz *et al.*, "A review of drug delivery systems for capsule endoscopy," *Adv. Drug Deliv. Rev.*, vol. 71, pp. 77–85, 2014.

[30] W. Yu *et al.*, "A smart capsule with GI-tract-location-specific payload release," *IEEE Trans. Biomed. Eng.*, vol. 62, no. 9, pp. 2289–2295, 2015.

[31] L. de Ridder, M.M. Tabbers, and J.C. Escher, "Small bowel endoscopy in children," *Best. Pract. Res. Clin. Gastroenterol.*, vol. 26, no. 3, pp.337-345, 2012.

[32] T. Okamoto and S. Okabe, "Ultraviolet absorbance at 260 and 280 nm in RNA measurement is dependent on measurement solution," *Int. J. Mol. Med.*, vol. 5, no. 6, pp. 657–659, 2000.

[33] S. Claassen *et al.*, "A comparison of the efficiency of five different commercial DNA extraction kits for extraction of DNA from faecal samples," *J. microbiol. M.*, vol. 94, no. 2, pp.103-110, 2013.

[34] M. Reck *et al.*, "Stool metatranscriptomics: A technical guideline for mRNA stabilisation and isolation," *BMC gen.*, vol.16, no. 1, p.494, 2015.

[35] *Browse All Products*, illumina, 2020. [Online]. Available: https://www.illumina.com/products/all-products.html

[36] J. Flemming *et al.*, "Small bowel capsule endoscopy," *Medicine*, vol. 97, no. 14, 2018

[37] F. Carpi *et al.*, "Controlled navigation of endoscopic capsules: concept and preliminary experimental investigations," *IEEE Trans. Biomed. Eng.*, vol. 54, no. 11, pp. 2028–2036, 2007.

[38] M. Sitti, *Mobile Microrobotics*. Cambridge, USA: MIT Press, 2017.

[39] S. H. Ku *et al.*, "General functionalization route for cell adhesion on non-wetting surfaces," *Biomaterials*, vol. 31, no. 9, pp. 2535–2541, 2010.

[40] V. Paget, "Specific uptake and genotoxicity induced by polystyrene nanobeads with distinct surface chemistry on human lung epithelial cells and macrophages," *PloS one*, vol. 10, no. 4, p. 01232972015, 2015.

[41] E. P. Furlani, *Permanent magnet and electromechanical devices: materials, analysis, and applications*. San Diego, CA, USA: Academic Press, Sep. 2001.

[42] D. Brown. (Sep. 2017). Tracker. [Online]. https://physlets.org/tracker/

[43] D. K. Owens and R. C. Wendt, "Estimation of the surface free energy of polymers," *J. Appl. Polym. Sci.*, vol. 13, no. 8, pp. 1741–1747, 1969.

[44] J. Curtis and A. Colas "Medical applications of silicones," in *Biomater. Sci.*, Academic Press, pp. 1106–1116, 2013.

[45] E. T. Hillman *et al.*, "Microbial Ecology along the Gastrointestinal Tract," *Microbes Environ*. vol. 32, no. 4, pp. 300–313, 2017.

[46] *The care and use of farm animals in research, teaching and testing*, Canadian Council on Animal Care, Ottawa, Canada, pp. 12–15, 2009.

[47] M. Gao *et al.*, "Design and fabrication of a magnetic propulsion system for self-propelled capsule endoscope," *IEEE Trans. Biomed. Eng.*, vol. 57, 2010.

[48] S. Park *et al.*, "Multi-functional capsule endoscope for gastro-intestinal tract," in *SICE-ICASE Int. Conf.*, Busan, Korea, 2006, pp. 2090–2093.

[49] L. A. Houghton *et al.*, "Motor activity of the gastric antrum, pylorus, and duodenum under fasted conditions and after a liquid meal," *Gastroenterology*, vol. 94, no. 6, pp. 1276–1284, 1988.

[50] X. Liu *et al.*, "Ingestible hydrogel device," *Nat. Comm.*, vol. 10, no. 1, p. 493, 2019.

[51]. H. Mateen *et al.*, "Localization of wireless capsule endoscope: A systematic review," *IEEE Sensors J.*, vol. 17, no. 5, pp. 1197–1206, 2017.

Peyman Shokrollahi received his B.Eng. in electrical engineering from Shiraz University, Shiraz, Iran in 2001, M.A.Sc. in electrical and computer engineering from Ryerson University, Toronto, Ontario, Canada in 2009, and Ph.D. in biomedical engineering from the University of Toronto, Toronto, Ontario, Canada in 2017. From 2012 to 2017, his research was on a magnetic resonance imaging compatible surgical robot for pediatric bone biopsy in collaboration with the Hospital for Sick Children (SickKids). From 2017 to 2019, he collaborated with SickKids to develop a microrobot for sampling microbiomes. Currently, he is a research scholar at Stanford University to develop an AI system for medical imaging protocols.

Yung P. Lai received the B.A.Sc. and M.A.Sc. in chemical engineering at the University of Waterloo, Waterloo, ON, Canada, in 2013 and 2015, respectively. She joined the Microrobotics Laboratory at the University of Toronto, Toronto, ON, Canada, in 2018, where she is currently a Ph.D. student. Her interests are in soft actuators and capsule endoscopy.

Samrand Rash-Ahmadi was born in Mahabad, Iran in 1976. He is an Associate Professor at the Mechanical Engineering of Urmia University. He joined Urmia University in 2008 after he received his Ph.D. degree in Solid Mechanics from Amirkabir (Polytechnic) University. He promoted to an Associate Professor in 2014. He is currently involved in scientific and didactic research in the fields of Solid Mechanics with focus on Computational Mechanics and Mechanics of Micro- and Nano Structures and Nano Composites.

Victoria Stewart received her B.S. in animal biology with a minor nutraceutical and nutritional sciences in 2016 at the University of Guelph, Ontario, Canada. She continued at Guelph to complete her M.S. in animal biosciences focusing on swine nutrition. In 2020, she started working as a Monogastric Nutritionist at Molesworth Farm Supply Ltd.

Mohsen Mohammadigheisar received a B.S. and M.S. in animal science from Islamic Azad University, Saveh, Iran, in 2010, and a Ph.D. in animal science from Dankook University, Cheonan, South Korea, in 2016. In 2017, he started working as a postdoctoral fellow in animal nutrition at the University of Guelph, Guelph, ON, Canada. His research interest includes the development of in-feed antibiotic alternatives, gut health, gut microbiome, and epigenetics.

Lee-Anne Huber received a B.S. degree in animal biology from the University of Guelph, Ontario, Canada in 2010 and a M.S. degree in swine nutrition from the same university in 2012. In 2016, she completed a Ph.D. degree in swine nutrition and metabolism from the University of Guelph after implementing a joint research program with Michigan State University, East Lansing, MI, USA. After a one-year post-doctoral fellowship at Memorial University of Newfoundland, St. John's, Newfoundland, Canada, she rejoined the University of Guelph as an Assistant Professor in the Department of Animal Biosciences. Dr. Huber's research interests include amino acid metabolism, nutrient partitioning, and digestive physiology in swine, as well as the use of pigs as models for human nutrition research. Dr. Huber is an Associate Editor for the Journal of Animal Science and a professional member of the American and Canadian Societies of Animal Science.

Naomi Matsuura received the B.A.Sc. and the M.A.Sc. degrees in Engineering Physics from Queen's University, Kingston, Canada, and the Ph.D. degree in Materials Science and Engineering from the University of Toronto, Toronto, Canada. She was a Postdoctoral Researcher and later a Research Associate at Sunnybrook Research Institute, Toronto, Canada. In 2014, she became an Assistant Professor in the Department of Medical Imaging, University of Toronto, Canada and since 2016, has been an Associate Professor in Materials Science and Engineering and Biomedical Engineering at the University of Toronto, Canada. Her current research interests include the development of new materials that interact specifically with medical imaging radiation for minimally invasive, image-guided and site-specific diagnosis and treatment of disease.

Anna E. H. Zavodni received the B.H.Sc. and M.D. degrees from the University of Alberta, Edmonton, in 2004 and 2005, respectively. She received a M.H.Sc. in Clinical Research from Duke University, Durham, NC, in 2011. From 2010 to 2011, she was a Clinical Fellow at the National Institutes of Health, Clinical Center, Department of Imaging Sciences. From 2012 to 2016, she was an Assistant Professor with the Department of Medical Imaging, University of Toronto. She is the author of 3 book chapters and more than 25 peer-reviewed papers. Her research interest includes advanced cardiovascular imaging.

John Parkinson received his BSc in Applied Biology from the University of Bath, UK in 1990 and his PhD degree in Biochemistry from the University of Manchester, UK in 1995. He is currently a Senior Scientist at the Hospital for Sick Children, Toronto, Canada and Full Professor in the Departments of Biochemistry and Molecular Genetics at the University of Toronto. Having helped author over 110 articles, Dr Parkinson's research focuses on the application of computational approaches to study microbial pathogenesis, as well as understanding how complex microbial communities contribute to health and disease. He is an Associate Editor of Microbiome.

Eric Diller received the B.S. and M.S. degree in mechanical engineering from Case Western Reserve University in 2010 and the Ph.D. degree in mechanical engineering from Carnegie Mellon University in 2013. He is currently Associate Professor and Dean's Catalyst Professor in the Department of Mechanical and Industrial Engineering at the University of Toronto, where he is director of the Microrobotics Laboratory. His research interests include micro-scale robotics, and features fabrication and control relating to remote actuation of micro-scale devices using magnetic fields, micro-scale robotic manipulation, smart materials. He is an Associate Editor of the Journal of Micro-Bio Robotics and received the award for Best Associate Editor at the 2015 IEEE International Conference on Automation and Robotics, as well as the IEEE Robotics & Automation Society 2020 Early Career Award. He has also received the 2018 Ontario Early Researcher Award, the University of Toronto 2017 Connaught New Researcher Award, and the Canadian Society of Mechanical Engineering's 2018 I.W. Smith Award for research contributions in medical microrobotics.